ARTICLES SCIENCE CHINA Materials

mater.scichina.com link.springer.com

Published online 5 September 2017 | doi: 10.1007/s40843-017-9089-y
Sci China Mater 2017, 60(10): 918–928

Acid promoted Ni/NiO monolithic electrode for overall water splitting in alkaline medium

Caicai Li[1], Junxian Hou[2], Zexing Wu[1], Kai Guo[1], Deli Wang[1], Tianyou Zhai[1] and Huiqiao Li[1*]

ABSTRACT Exploring and designing bi-functional catalysts with earth-abundant elements that can work well for both hydrogen evolution reaction (HER) and oxygen evolution reaction (OER) in alkaline medium are of significance for producing clean fuel to relieve energy and environment crisis. Here, a novel Ni/NiO monolithic electrode was developed by a facile and cost-effective acid promoted activation of Ni foam. After the treatment, this obtained monolithic electrode with a layer of NiO on its surface demonstrates rough and sheet-like morphology, which not only possesses larger accessible surface area but also provides more reactive active sites. Compared with powder catalysts, this monolithic electrode can achieve intimate contact between the electrocatalyst and the current collector, which will alleviate the problem of pulverization and enable the stable function of the electrode. It can be served as an efficient bi-functional electrocatalyst with an overpotential of 160 mV for HER and 290 mV for OER to produce current densities of 10 mA cm^{-2} in the alkaline medium. And it maintains benign stability after 5,000 cycles, which rivals many recent reported noble-metal free catalysts in 1.0 mol L^{-1} KOH solution. Attributed to the easy, scalable methodology and high catalytic efficiency, this work not only offers a promising monolithic catalyst but also inspires us to exploit other inexpensive, highly efficient and self-standing noble metal-free electrocatalysts for scale-up electrochemical water-splitting technology.

Keywords: electrocatalysis, bi-functional, acid promoted activation, Ni/NiO, water splitting, monolithic electrode

INTRODUCTION

Water electrocatalysis for clean fuel production is an appealing solution to meet the ever-growing energy demands at no environmental cost [1–4]. And the great demand of H_2 production triggers a body of research inputs on the water splitting, in which the key fact depends on the innovative exploitation regarding the design of efficient electrocatalysts helping lower the overpotential meanwhile obtaining decent reaction rates [5,6]. However, the most efficient noble-metal based electrocatalysts suffer from natural resource scarcity and high-cost, which hampers their broad utilization [7–10]. Although a variety of non-noble metal-based nanostructured materials such as Mo_2C/MoO_2 [11], Co_9S_8/graphene [12], CoPS [13], CoMoS [14], NiMoN [15] have been reported, the facts are still far from satisfactory since these materials are either for oxygen evolution reaction (OER) catalysts working in strongly alkaline conditions or for hydrogen evolution reaction (HER) catalysts operating in strongly acidic mediums due to the thermodynamic convenience [5,16–18]. The inferior efficiency caused by the disparity of the stability and activity for the same catalyst system in the operating pH ranges [19,20] limits the practical implementations of these materials as a catalytic electrode in an integrated electrolyser. Therefore, a formidable challenge for electrocatalytic water splitting is to explore and design bifunctional catalysts that can work well for both HER and OER in the same alkaline medium to accomplish overall water splitting.

Up to now, several types of bifunctional materials such as metal oxides [21], phosphides [22] and nitrides [23] have been explored as earth-enriched electrocatalysts for overall water splitting. However, the fabrication of these powder catalysts usually involves tedious and complicated steps to get desirable nanostructures. And the obtained catalysts have to be further loaded onto specific current collector for subsequent performance tests. During the

[1] State Key Laboratory of Material Processing and Die & Mould Technology, School of Materials Science and Engineering, School of Chemistry and Chemical Engineering, Huazhong University of Science and Technology (HUST), Wuhan 430074, China
[2] Department of Composite Materials and Engineering, College of Materials Science and Engineering, Hebei University of Engineering, Handan 056038, China
* Corresponding author (email: hqli@hust.edu.cn or huiqiaoli@gmail.com)

loading process, it is difficult to achieve highly dispersion of the catalysts over the electrode surface. And the contact between the electrocatalysts and the current collector is not so intimate by this post-loading method [24]. As a result, the pulverized catalysts tend to peel off from the substrate especially in a working circumstance where lots of hydrogen and oxygen would continuously bubble up, leading to gradually decreased catalytic efficiency as well as limited life span [25]. In comparison, growing the catalysts directly onto the conductive substrate such as Ni foam (NF) [26,27], carbon cloth [28,29], carbon fiber paper [30] and Ti foil [31] can mitigate the problem of falling off and contact to some extent. However, the matter of the contact interface between electrocatalysts and the current collector as well as pulverization issues is still not fully addressed. Therefore, exploring monolithic electrodes towards HER and OER consisting of a current collector immobilized with noble-metal-free catalysts [24] to enhance the durability of the catalysts remains challenging.

NF, a widely used electrode that serves as a promising substrate for the support of many catalysts, possesses unique features such as good electrical conductivity, intrinsic strength, corrosion resistance, high surface area and low cost [26,32]. However, the intrinsic activity of metallic nickel towards HER or OER under alkaline conditions is not so good. Here, we successfully developed an integrated electrode based on metallic NF with robust electrocatalytic properties by a facile acid-promoted activation process. Benefiting from the increased accessible surface area and active sites, the novel acid-activated electrode presents considerable activity and alkaline-stability toward the HER and OER. Specifically, the obtained electrode demonstrates the overpotentials of 160 mV for HER and 290 mV for OER to produce current density of 10 mA cm^{-2} and exhibits high tolerance and durability under harsh basic conditions, which enables it comparable to the reported noble metal-free catalysts. Additionally, compared with other 3D electrodes with excellent electrochemical performance, such as WSe_2 [33], np-Co_2P [34], CP/CTs/Co-S [35], this acid activation process of 3D NF electrode has the advantages of simplicity, low cost and mass-production. Compared with traditional powder catalysts, the 3D monolithic electrode with decent catalytic stability is actually preferable for practical use by tailoring the size of the electrode to adapt to different electrochemical devices. This work may pave a viable way of fabricating cheap and highly efficient electrodes for the electrochemical water splitting technology.

EXPERIMENTAL SECTION

Sample preparation

All reagents were directly used without any further purification. The activated NF (ANF) was obtained by an acid promoted activated process. Briefly, prior to activation, NF was cut into pieces (2 cm×3 cm) and cleaned with distilled water and ethanol in turn and then left dry in air. Afterwards, a few pieces of NF were directly immersed into 200 mL of 3 mol L^{-1} HCl aqueous solution which was heated on a hotplate at the setting temperatures of 60, 90, 120 and 150°C, respectively, for different time (10, 20, 30 and 40 min). And the corresponding inner temperature of HCl solution was tested to be about 50, 60, 70 and 80°C. In this paper, all the activation temperature refers to the value of hotplate, not that of the HCl solution. Then, the ANF was removed and cleaned with distilled water to remove any extra HCl solution. Finally, the ANF was dried at room temperature for further experiments.

Material characterization

X-ray diffraction (XRD) data of the activated samples were obtained by using a PANalytical B.V. Empyrean diffractometer. The morphology and microstructure of the samples were observed by scanning electron microscopy (SEM, FEI Sirion 650). The elemental analysis was investigated using X-ray photoelectron spectroscopy (XPS, Thermo Fisher ESCALAB 250.)

Electrochemical measurements

The electrochemical performances were carried out on a typical three-electrode electrochemical cell using a CHI 760e electrochemistry workstation (Chenhua, Shanghai) with an electrolyte solution of 1.0 mol L^{-1} KOH The obtained Ni/NiO electrode served as the working electrode with a graphite rod counter electrode and a Hg/HgO (in 1.0 mol L^{-1} KOH) reference electrode. Before each measurement, the electrolyte was purged by ultra-high pure nitrogen (> 99.999%) at least for 30 min, and the N_2 bubbling was then maintained over the entire duration of the electrochemical experiments. The polarization curves of the HER and OER were conducted in electrolyte with a scan rate of 5 mV s^{-1}. The cyclic voltammetry (CV) plots used to probe the electrochemical double layer capacitance at non-faradaic potential to estimate the effective electrode surface area were swept between 0.6 and 0.75 V in 1.0 mol L^{-1} KOH with the scanning rates of 20, 40, 60, 80 and 100 mV s^{-1}. Current density-time (*i*-*t*) curves were measured for characterizing the stability of HER, OER and overall water splitting in 1.0 mol L^{-1} KOH. The ac-

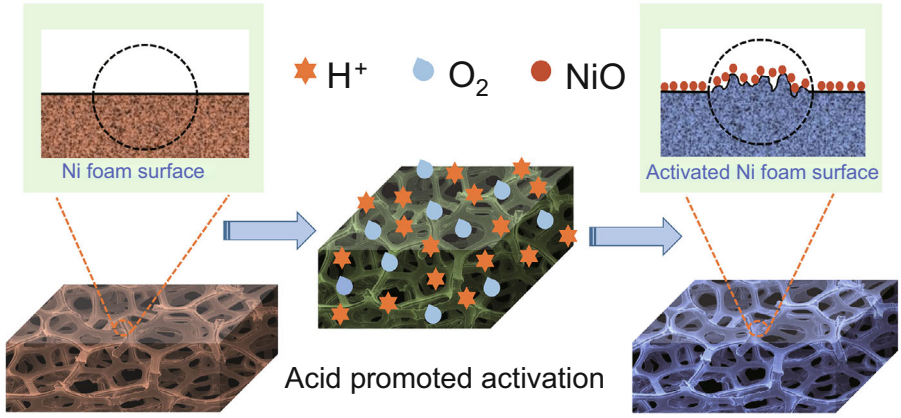

Figure 1 Schematic illustration of the activation process to prepare the monolithic Ni/NiO electrode.

celeration degradation test (ADT) was conducted by 5,000 potential cycling under corresponding HER or OER region at a scan rate of 100 mV s^{-1}. Electrochemical impedance spectroscopy (EIS) was performed by scanning the frequency from 10^5 to 0.01 Hz at −0.1 V *vs.* reversible hydrogen electrode (RHE) with an amplitude of 5 mV. For overall water splitting, electrochemical measurements were carried out in a two-electrode setup in 1.0 mol L^{-1} KOH solution using ANF as the anode and cathode. All displayed voltammetry were iR-corrected to account for any uncompensated resistance. The uncompensated resistance was measured by EIS. The calculation of current densities was based on the actual area of electrode that was immersed in the electrolyte and the height of electrode was carefully adjusted. All the potentials measured in our work were calibrated with RHE according to the equation: $E_{RHE} = E_{Hg/HgO} + 0.0591pH + 0.098$.

RESULTS AND DISCUSSION

A schematic representation of the activated process of NF is shown in Fig. 1. In short, a few pieces of NF (2 cm× 3 cm) were soaking into the 3 mol L^{-1} HCl solution at different temperatures for different time, respectively (see EXPERIMENTAL SECTION for the detailed process). During the acid treatment process, the surface Ni was first dissolved in 3 mol L^{-1} HCl solution, which can be seen from the color changes of the solutions (Fig. S1). Subsequently, the newly exposed highly reactive surface was prone to be oxidized by the dissolved oxygen in the solution and the oxygen in the air to form a new nickel oxide layer. The morphology and the microstructure of NF and ANF electrode or Ni/NiO electrode were acquired by SEM and the results are demonstrated in Fig. 2. From the SEM images of Fig. 2a, c, e, it can be seen that the surface of pristine NF is smooth in general though a bit

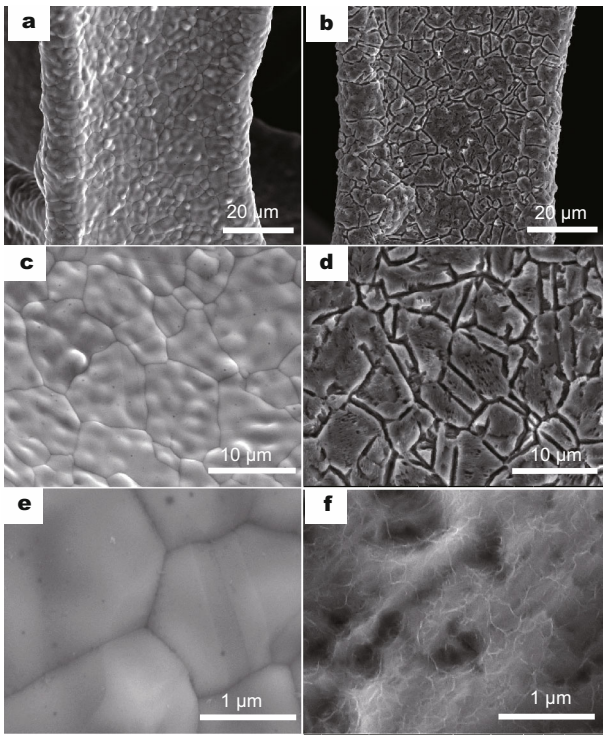

Figure 2 SEM images of bare NF (a, c, e) and the obtained Ni/NiO electrode for activating the NF at 120°C for 30 min (b, d, f).

uneven, whereas the NF becomes rough and numerous ravines and even some pores are formed after the acid treatment (Fig. 2b, d). SEM image (Fig. 2f) with higher magnification reveals that a layer of sheet-like structure is formed after the acid treatment process. Furthermore, with the increase of the activation temperature from 60 to 120°C and longer treatment time from 10 to 30 min (higher temperature and time will lead the NF to be corroded and broken, see Fig. S2), the NF would be

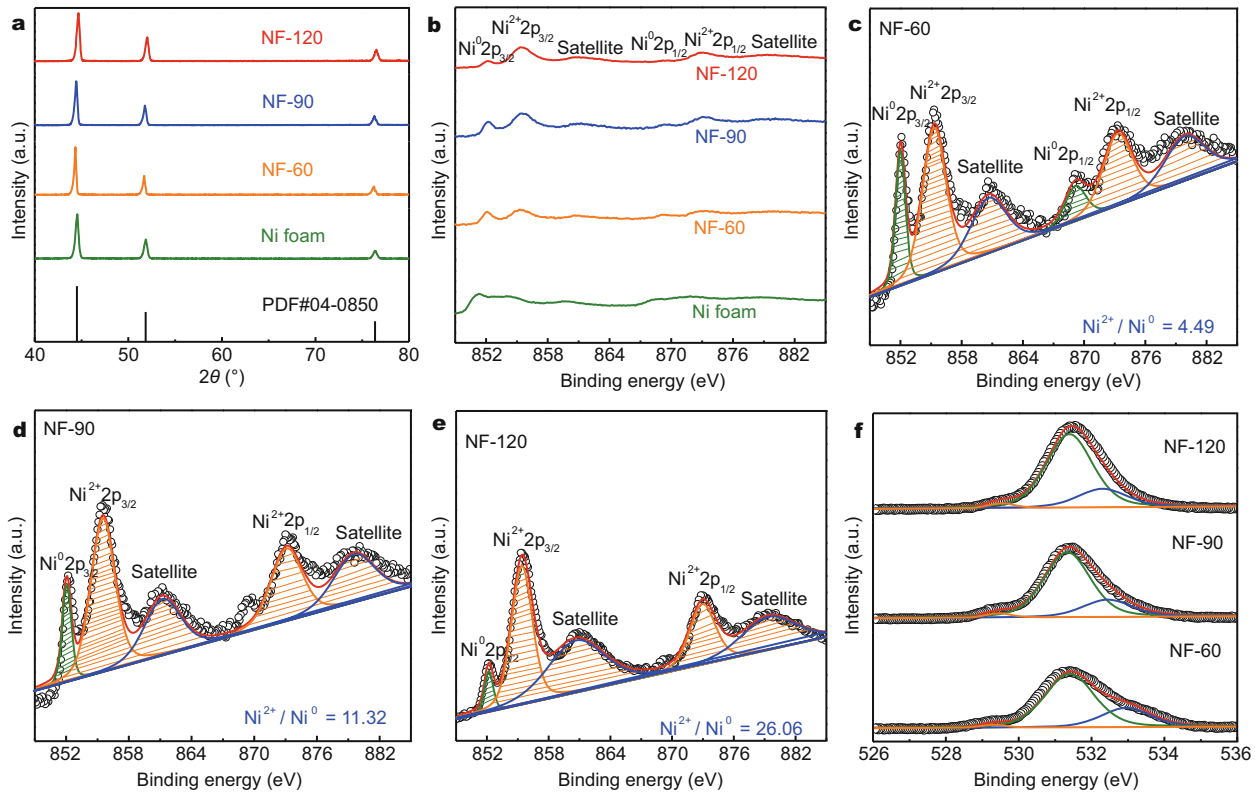

Figure 3 XRD and XPS analyses of the obtained Ni/NiO electrodes with NF treated at different temperatures. (a) XRD patterns. (b) XPS spectra of Ni 2p. (c–e) The fitting of the peak areas of Ni^{2+} and Ni^{0}. (f) XPS spectra of O 1s.

etched more seriously and form more rough surface (Fig. S3).

XRD and XPS were carried out to identify the elemental composition and valence state before and after acid-treatment. As displayed in Fig. 3a, only the signals of metallic nickel are observed because the formation of NiO on the surface of NF was too little to be detected. Fig. S4a, b show the typical XPS survey spectra of NF and Ni/NiO obtained at different temperatures and time. All spectra were calibrated with the C 1s peak to 284.8 eV. Only signals of Ni, O and C elements are observed, which indicates that no other impurities were introduced during the activation process. The Ni 2p core-level XPS spectra are displayed in Fig. 3b, in which two Ni 2p core levels ($2p_{1/2}$ and $2p_{3/2}$) and two satellite peaks are observed. The binding energy separation between core levels Ni $2p_{1/2}$ (872.95 eV) and Ni $2p_{3/2}$ (855.39 eV) is 17.56 eV, which matches with electronic states of NiO [36]. While the peaks located at 852.0 and 869.15 eV are associated with the typical binding energies for Ni $2p_{3/2}$ and Ni $2p_{1/2}$ of Ni^{0} [37] respectively. Meanwhile, compared with the pristine NF, the Ni 2p intensities of the Ni^{2+} peaks of Ni/NiO samples become stronger with the increase of activated temperatures, which indicates the increased amount of nickel oxide on the surface of ANF. Furthermore, the corresponding lower intensity of the characteristic Ni^{0} peaks also validates the generation of nickel oxide on the ANF surface. In order to further clearly exhibit the activated promoted self-growth of NiO on the NF surface at the increased activated temperatures, we fitted the peak areas of the Ni 2p and then calculated the proportion of Ni^{2+}/Ni^{0}. From Fig. 3c–e, it can be concluded that the value of the Ni^{2+}/Ni^{0} varies from 4.49 to 26.06, which further confirms the above conclusion. In the O 1s spectra (Fig. 3f), the peak at 529.5 eV reveals the existence of Ni–O–Ni bond, which is consistent with NiO electronic state, and the peak at 531.6 eV is attributed to oxygen vacancies, while the peak at 532.5 eV may be due to the adsorbed water or possibly adsorbed O_2 [38,39]. In addition, the O 1s peak intensity of the Ni/NiO sample gradually increases with the increasing activated temperatures (Fig. S5), which further proves the formation of NiO on the NF surface due to the acid activation process. In addition to the temperature, activation time may also influence the formation of surface NiO, so conditional experiments were conducted for different activation time. Similar re-

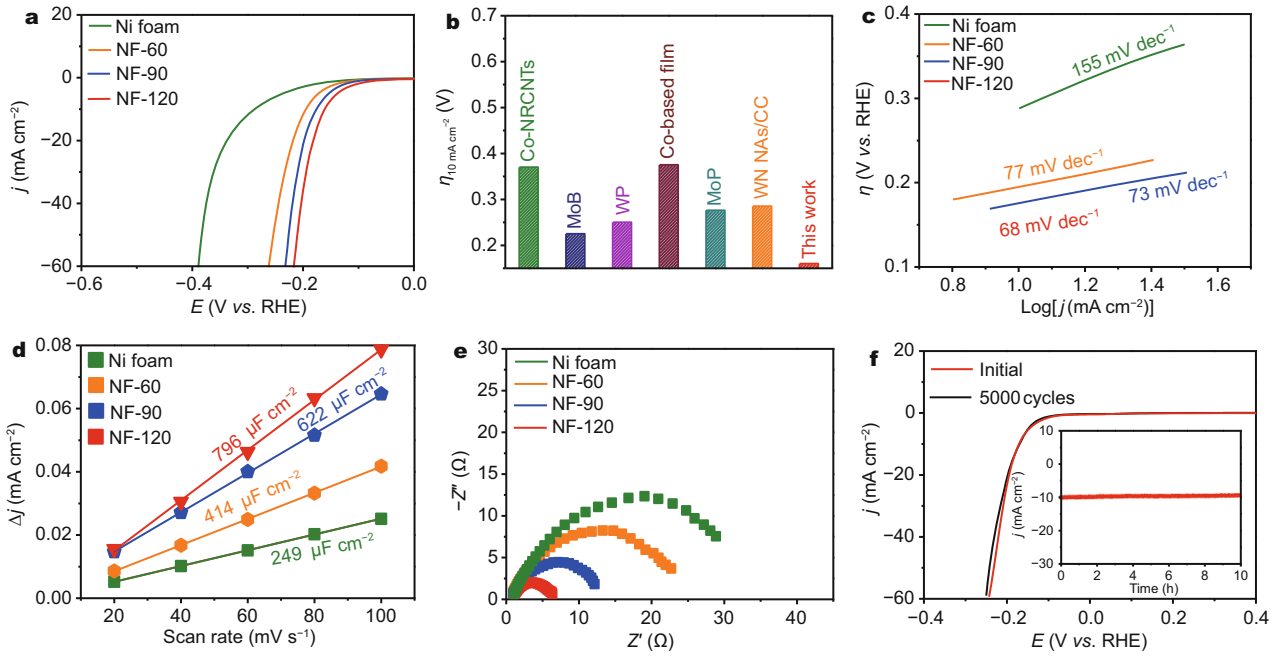

Figure 4 (a) Linear sweep voltammetry (LSV) curves for bare NF and Ni/NiO obtained at different temperatures (60, 90, 120°C) with a scan rate of 5 mV s^{-1} for HER in 1.0 mol L^{-1} KOH. (b) Comparison of overpotential for Ni/NiO with other reported noble-metal free catalysts. (c) Tafel slopes for different Ni/NiO samples. (d) Plots of capacitive currents as a function of scan rate for Ni/NiO obtained at different temperatures. (e) Nyquist plots of the different Ni/NiO catalysts in 1.0 mol L^{-1} KOH. (f) LSV curves for NF-120 before and after 5,000 CV cycles, and the inset is the corresponding time-dependent current density curve under a static overpotential.

sults are exhibited in Fig. S6, where increasing the activation time does not change the main composition of the products (Fig. S6a) and the peak intensities of Ni^{2+} 2p and O 1s also increase with the increase of the activation time (Figs S6 and S7). The combination of XRD and XPS measurement results indicate that the activated NF has a core of Ni and some NiO on its surface.

The electrocatalytic properties of the Ni/NiO electrode were firstly studied by HER in strong alkaline solution using a typical three-electrode setup. Fig. 4a presents the representative polarization curves (with iR compensation). As can be clearly seen, bare NF possesses quite weak catalytic activity, while in sharp contrast, all the Ni/NiO samples display enhanced HER performance, implying that the activation process can effectively improve the HER catalytic properties of NF. In addition, the NF-120 exhibits remarkably high activity with an onset potential of ~73 mV and an overpotential of 160 mV *vs.* RHE at the current density of 10 mA cm^{-2} (NF-60, NF-90 and the bare NF display overpotentials of 195, 176 and 288 mV, respectively). This overpotential is comparable to or even smaller than those of many reported values for non-Pt HER catalysts in basic aqueous media, including Co-NRCNTs (370 mV) [40], MoB (225 mV) [41], WP (250 mV) [28], porous Co-based film (375 mV) [42], MoP (276 mV) [43], and WN NAs/CC (285 mV) [44], (see Fig. 4b and Table S1 in the Supplementary information for more details). The influence of activation time on the catalytic properties of the Ni/NiO electrode is depicted in Fig. S8a. It is apparent that with the increased activation time from 10 to 30 min, the overpotential of the Ni/NiO decreases from 196 to 160 mV. All these results showed that the NF-120 (30 min) exhibited higher catalytic activity than other samples. Given the facts above, we proposed that the enhanced HER catalytic activity may be due to the following reasons: (1) the metallic Ni substrate with excellent conductivity enables it to transport charge and electron effectively. (2) Intimate contact between the Ni substrate and electrochemically active NiO reduces the interface resistance and facilitates the interfacial charge transfer. (3) The Ni/NiO electrode with rough surface contributes to larger accessible surface area, which is favorable for enhancing the electrolyte-material contact area and providing more reactive sites for the improvement of HER performance.

The linear regions of the Tafel plots (Fig. 4c and Fig. S8b) were fitted into the Tafel equation ($b\log(j) + a$, where b is the Tafel slop and j is the current density), yielding 68 mV dec^{-1} for NF activated at 120°C for 30 min. This further indicates that NF-120 has better

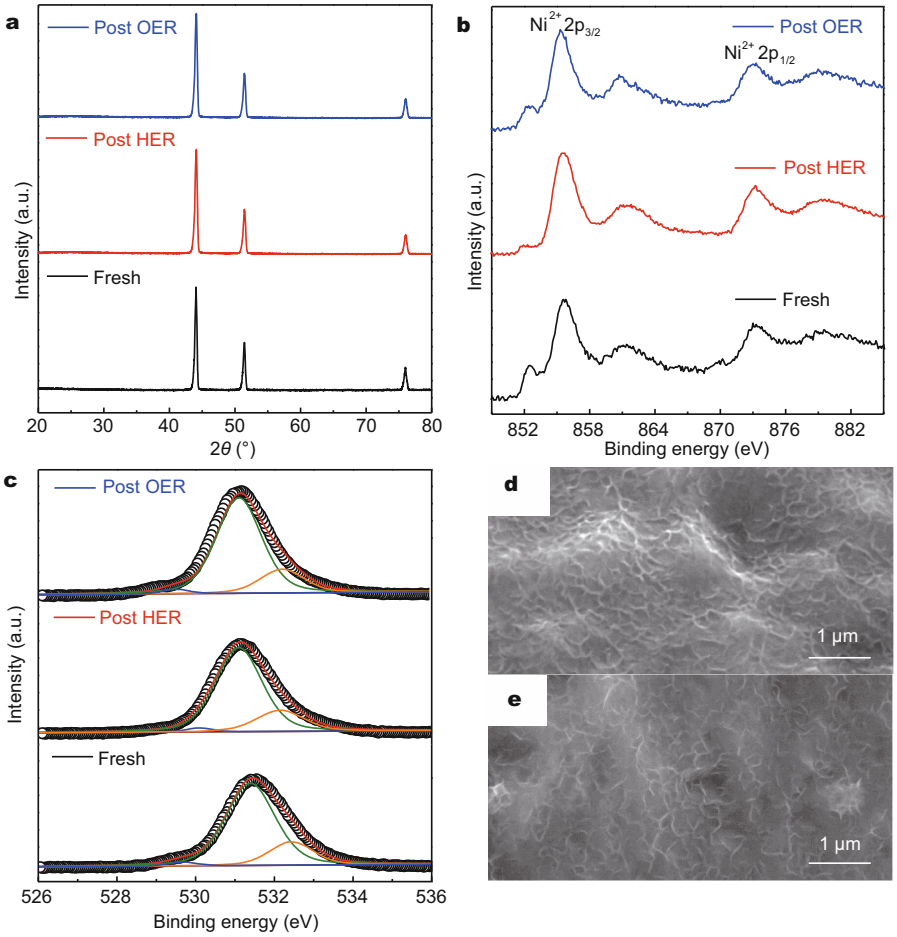

Figure 5 (a) XRD pattern; (b) XPS spectra of Ni 2p and (c) XPS spectra of O 1s for the fresh, post HER and post OER Ni/NiO sample activated at 120°C for 30 min. SEM images of NF-120 after a 10 h HER (d) and OER (e) stability test.

catalytic performance and rivals the performance of many basic-stable HER catalysts, such as NiCoP/rGO (b = 124.1 mV dec^{-1}) [45], CP/CTs/Co-S (b = 131 mV dec^{-1}) [35], MoS_2 nanosheets (b = 100 mV dec^{-1}) [46], and FeP NWs (b = 75 mV dec^{-1}) [47], (see Table S1 for more details). Generally, a Tafel slope of 116, 38, and 29 mV dec^{-1} was expected if the rate-determining step in HER was Volmer, Heyrovsky, and Tafel reactions, respectively [48]. Thus the experimentally observed Tafel slope of 68 mV dec^{-1} for NF-120 implies that hydrogen evolution behavior occurring on the surface follows a Volmer–Heyrovsky mechanism. The lowest overpotential and smallest Tafel slope (Fig. 4a, c) for NF-120 imply its superior HER activity.

The CV measurement with different scan rates was employed to evaluate the double-layer capacitance (C_{dl}) at the solid/liquid interface of all electrodes for better comparison of the activity of Ni/NiO described here [49,50]. C_{dl} was linearly proportional to the effective active surface area [51], and it could be estimated by plotting the Δj (j_a - j_c) at 0.67 V *vs.* RHE against the scan rate, where the slope was twice as the C_{dl}. The CVs were collected in the region of 0.62 ~ 0.72 V (*vs.* RHE), where the current response comes only from the charging of the double layer (Figs S9 and S10), and the linear slope of the capacitive current against scan rate was used to represent the electrochemically active surface area. From Fig. 4d and Fig. S8c, it is clearly that the C_{dl} of NF-120 (398 μF cm^{-2}) is higher than other Ni/NiO electrodes obtained at different activation conditions. This suggests that increasing activation temperature and treatment time will create more exposed active sites in the Ni/NiO series, which is beneficial to the enhanced HER activity.

EIS was performed to shed light on the HER kinetics and interface reactions on the surface of the catalysts. Nyquist plots (Fig. 4e and Fig. S8d) reveal an obviously

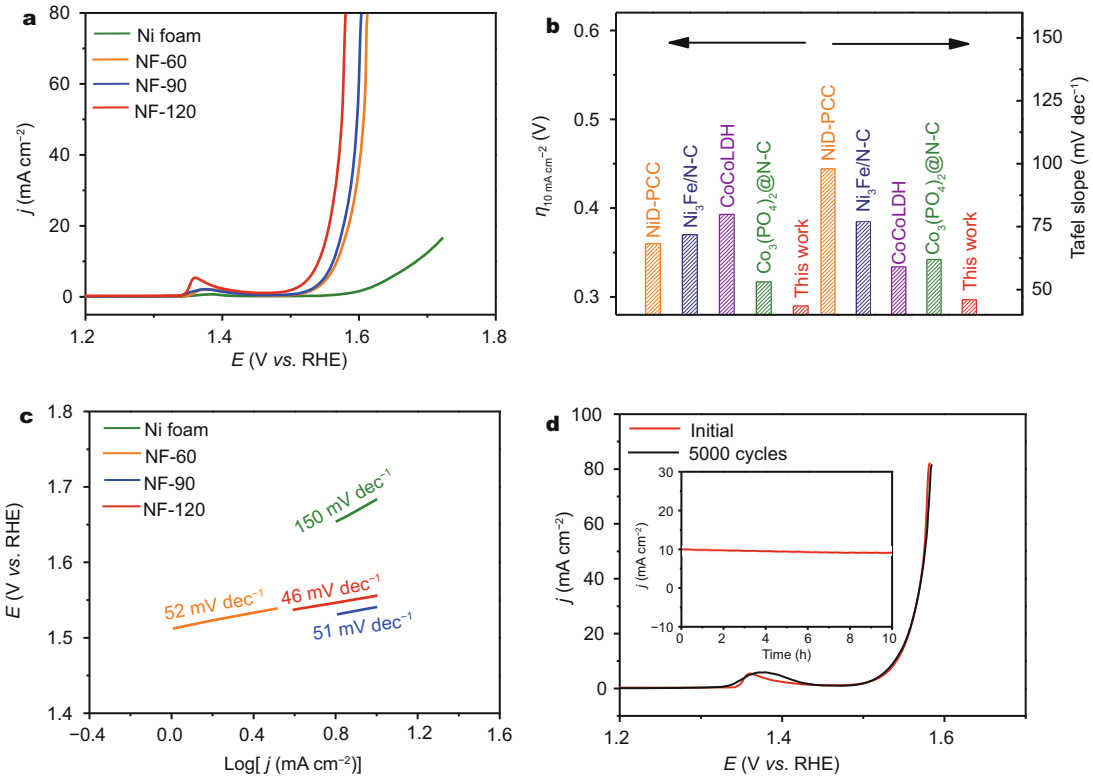

Figure 6 (a) LSV curves for bare NF and the obtained Ni/NiO at different temperatures (60,90,120°C) with a scan rate of 5 mV s^{-1} for OER in 1.0 mol L^{-1} KOH. (b) Comparison of the overpotential and Tafel slope for Ni/NiO with other reported noble-metal free catalysts. (c) Tafel slopes for different Ni/NiO samples. (d) LSV curves of NF-120 catalysts in 1.0 mol L^{-1} KOH before and after long-term 5,000 cycles, and the inset is the corresponding time-dependent current density curve at a static overpotential.

decreased charge transfer resistance after the acid-activation, which means more rapid charge transfer kinetics. The improved charge transfer ability could promote the combination of electrons and Hads, and benefit the electrical integration to minimize concomitant Ohmic losses [52,53], and thus the electrocatalytic activity was enhanced. The good HER performance of Ni/NiO can be attributed to the low hydrogen adsorption impedance and fast charge-transfer kinetics on the surface of the electrode.

In addition to good catalytic activity, durability is also a key concern for all catalysts. After continuous CV scanning for 5,000 cycles in 1.0 mol L^{-1} KOH at a scan rate of 100 mV dec^{-1}, the polarization curve overlays almost exactly with the initial one (Fig. 4f). And the current density shows no apparent debasement for 10 h long time test (inset of Fig. 4f). Besides, XRD (Fig. 5a) and XPS analyses (Fig. 5b, c and Fig. S11) of this catalyst electrode suggest that after long period stability test, the main components of the catalyst are still nickel and oxide element though a slight decrease of NiO (the negligible lower intensity of the O 1s) owing to the electrochemical reduction (Fig. 5c and Fig. S11). SEM image (Fig. 5d) indicates that this catalyst electrode still maintains most of its morphology after 5,000 cycles. All these results confirm the stable performance of this self-standing non-noble HER electrocatalyst.

Besides HER performance, the activity of Ni/NiO for electrochemical oxidation of water to produce oxygen was also evaluated. Fig. 6a and Fig. S12a show the iR corrected polarization curves of the activated NF in an anodic direction. Similar to its HER performance, the activated NF displays obviously enhanced OER activity. Among the samples, NF-120 electrode by 30 min activation shows the best activity. The bare NF electrode shows poor OER activity, and the overpotential to generate 10 mA cm^{-2} is 450 mV. In contrast, the activated NF is highly active towards OER. With the changes of activation temperature and time, Ni/NiO electrodes deliver an overpotential varying from 350 (NF-60) to 290 mV (NF-120) for OER at the current density of 10 mA cm^{-2}. The peak at 1.35 V *vs.* RHE observed in Fig. 6a for Ni/NiO is ascribed to the

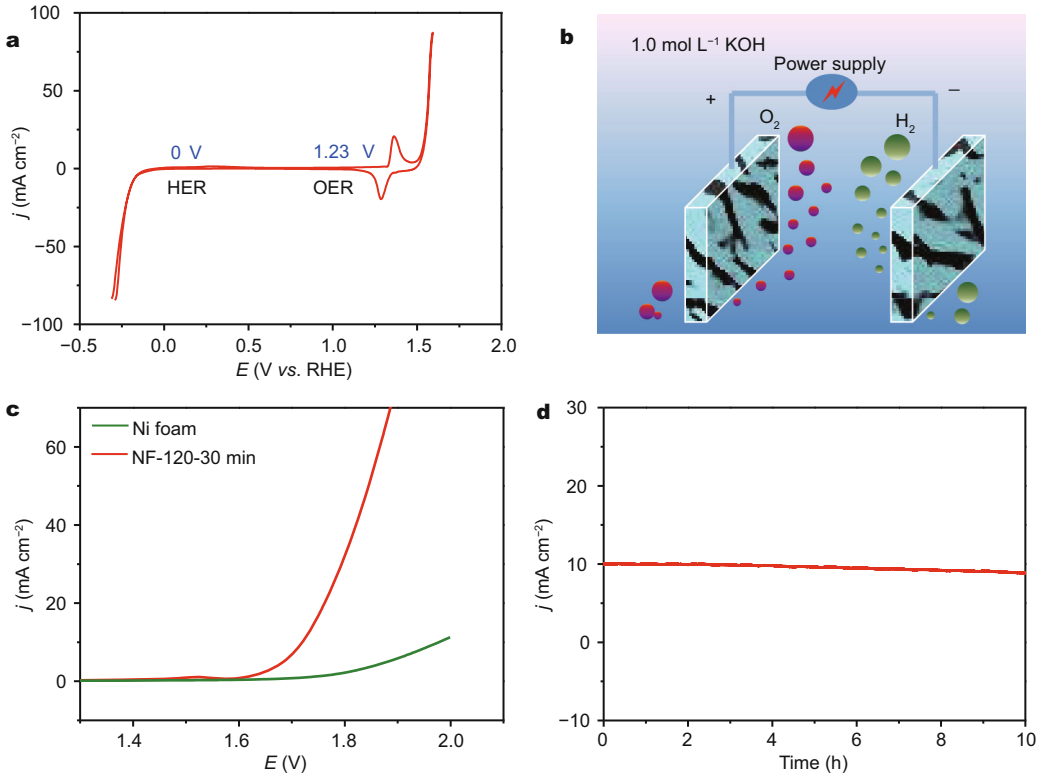

Figure 7 (a) CV curves of Ni/NiO obtained at 120°C in 1.0 mol L^{-1} KOH with a scan rate of 100 mV s^{-1}. (b) Schematic illustration of two-electrode cell using NF-120 for both anode and cathode for water splitting. (c) Current–potential response of an alkaline electrolyzer using NF-120 as catalyst for both OER and HER in 1.0 mol L^{-1} KOH. (d) Time dependence of catalytic current density during water electrolysis for NF-120 in 1.0 mol L^{-1} KOH at 1.72 V.

redox of Ni^{3+}/Ni^{2+}, which agrees with most of the reported Ni-based bifunctional electrocatalysts [54]. Tafel plots derived from polarization curves were conducted to evaluate the reaction kinetics (Fig. 6c and Fig. S12b). The resulting Tafel slope of NF-120 is 46 mV dec^{-1}, smaller than that of the other catalysts (51, 52, 53 and 63 mV dec^{-1} for NF-90, NF-60, NF-20 min and NF-10 min). This is a sign of more favorable kinetics with a more rapid oxygen evolution rate. The low overpotential and small Tafel slope underline the excellent oxygen evolution efficiency of NF-120, which rivals most the state-of-the-art non-noble metal OER catalysts working in alkaline media, such as NiD-PCC ($\eta_{10\ mA\ cm^{-2}}$ = 360 mV, b = 98 mV dec^{-1}) [55], Ni_3Fe/N-C ($\eta_{10\ mA\ cm^{-2}}$= 370 mV, b = 77 mV dec^{-1}) [56], CoCoLDH ($\eta_{10\ mA\ cm^{-2}}$= 393 mV, b = 59 mV dec^{-1}) [57], and $Co_3(PO_4)_2$@N-C ($\eta_{10\ mA\ cm^{-2}}$= 317 mV, b = 62 mV dec^{-1}) [58] (see Fig. 6b and Table S2 in the Supplementary information for more details). Additionally, continuous 5,000 cycles of CV scanning exhibits almost no degradation in current density (Fig. 6d). And the corresponding time-dependent current density curve presents only a slight degradation for 10 h (inset of Fig. 6d), which could be due to the hindrance of bubbles remaining on the surface of the electrode. To get more insight into the catalytic properties of the Ni/NiO electrode, the spent electrode after OER electrochemical test was further characterized by XRD and XPS. The XRD pattern reveals that the diffraction peaks of nickel from the used electrode are still retained (Fig. 5a), indicating excellent stability of Ni/NiO under the OER conditions. While the survey XPS spectrum exhibits that the Ni/NiO electrode still consists of Ni and O as the major components (Fig. S11), an increased amount of O appeared in the post-OER sample, likely arising from hydroxylation upon continuous OER electrolysis. Furthermore, the SEM image (Fig. 5e) of the spent OER catalyst still shows a rough surface similar to the fresh Ni/NiO sample, indicating remarkable structural robustness.

CV data recorded between −0.4 and 2.0 V (*vs.* RHE) reveals that the obtained NF electrode in this study is capable of acting as an efficient bifunctional HER and OER catalyst (Fig. 7a), which is in accordance with the

above analysis. With that in mind, an electrolyzer was conducted with the same catalyst both as the cathode and anode (NF-120||NF-120) for the electrochemical full water spitting in alkaline medium (Fig. 7b). As shown in Fig. 7c, the overall water-splitting of the NF-120 electrolyzer exhibits overall voltage of 1.72 V at 10 mA cm^{-2}, which is lower than the pristine NF electrolyzer due to the faster charge-transfer kinetics. In addition, the performance of this NF-120 electrode is comparable to some reported bifunctional catalysts, including CP/CTs/Co-S ($\eta_{10\ mA\ cm^{-2}}$= 1.74 V) [35], Ni_3S_2/NF ($\eta_{13\ mA\ cm^{-2}}$= 1.76 V) [59] and Co_x-PO_4/CoP ($\eta_{10\ mA\ cm^{-2}}$= 1.91 V) [42]. Furthermore, the NF-120 shows good stability upon continuous operation and only a slight deactivation is observed after 10 h (Fig. 7d), indicating excellent durability in long-term electrochemical process.

CONCLUSIONS

In conclusion, a facile acid-treatment process has been carried out to develop a monolithic Ni/NiO electrode for efficient electrochemical water spitting. After being immersed in HCl solution for 30 min, the effect of acid-etching not only results in the formation of a layer electrochemical active NiO on the electrode surface but also promotes the formation of rough and sheet-like morphology, which not only enhances the surface area but also facilitates the charge collection and transport. After acid treatment, the NF activated at 120°C for 30 min is found to show decent catalytic activity when used as a bifunctional electrocatalyst for both HER and OER compared to other self-supporting non-noble metal free catalysts. Small Tafel slopes (68 mV dec^{-1} for HER and 46 mV dec^{-1} for OER) and benign durability up to 10 h indicate excellent catalytic kinetics and enhanced stability. More importantly, this present activation process has the advantages of simplicity, low cost and scalable production in one activation process. Our work provides new ground to further expand the search for new electrocatalysts that do not contain expensive noble metals for applications.

Received 4 July 2017; accepted 3 August 2017; published online 5 September 2017

1 Turner JA. Sustainable hydrogen production. Science, 2004, 305: 972–974
2 Dresselhaus MS, Thomas IL. Alternative energy technologies. Nature, 2001, 414: 332–337
3 Gray HB. Powering the planet with solar fuel. Nat Chem, 2009, 1: 7–7
4 Lewis NS, Nocera DG. Powering the planet: chemical challenges in solar energy utilization. Proc Natl Acad Sci USA, 2006, 103: 15729–15735
5 Jiao Y, Zheng Y, Jaroniec M, *et al.* Design of electrocatalysts for oxygen- and hydrogen-involving energy conversion reactions. Chem Soc Rev, 2015, 44: 2060–2086
6 Zheng Y, Jiao Y, Zhu Y, *et al.* Hydrogen evolution by a metal-free electrocatalyst. Nat Commun, 2014, 5: 3783
7 Lu S, Zhuang Z. Electrocatalysts for hydrogen oxidation and evolution reactions. Sci China Mater, 2016, 59: 217–238
8 Chen WF, Sasaki K, Ma C, *et al.* Hydrogen-evolution catalysts based on non-noble metal nickel-molybdenum nitride nanosheets. Angew Chem Int Ed, 2012, 51: 6131–6135
9 Ledendecker M, Krick Calderón S, Papp C, *et al.* The synthesis of nanostructured Ni_5P_4 films and their use as a non-noble bifunctional electrocatalyst for full water splitting. Angew Chem Int Ed, 2015, 54: 12361–12365
10 Gong M, Zhou W, Tsai MC, *et al.* Nanoscale nickel oxide/nickel heterostructures for active hydrogen evolution electrocatalysis. Nat Commun, 2014, 5: 4695
11 Yang Y, Xu X, Wang X. Synthesis of Mo-based nanostructures from organic-inorganic hybrid with enhanced electrochemical for water splitting. Sci China Mater, 2015, 58: 775–784
12 Dou S, Tao L, Huo J, *et al.* Etched and doped Co_9S_8/graphene hybrid for oxygen electrocatalysis. Energ Environ Sci, 2016, 9: 1320–1326
13 Cabán-Acevedo M, Stone ML, Schmidt JR, *et al.* Efficient hydrogen evolution catalysis using ternary pyrite-type cobalt phosphosulphide. Nat Mater, 2015, 14: 1245–1251
14 Wu Z, Guo J, Wang J, *et al.* Hierarchically porous electrocatalyst with vertically aligned defect-rich CoMoS nanosheets for the hydrogen evolution reaction in an alkaline medium. ACS Appl Mater Interfaces, 2017, 9: 5288–5294
15 Zhang Y, Ouyang B, Xu J, *et al.* 3D porous hierarchical nickel-molybdenum nitrides synthesized by RF plasma as highly active and stable hydrogen-evolution-reaction electrocatalysts. Adv Energ Mater, 2016, 6: 1600221
16 Ma TY, Dai S, Jaroniec M, *et al.* Metal–organic framework derived hybrid Co_3O_4-carbon porous nanowire arrays as reversible oxygen evolution electrodes. J Am Chem Soc, 2014, 136: 13925–13931
17 Liu Q, Tian J, Cui W, *et al.* Carbon nanotubes decorated with CoP nanocrystals: a highly active non-noble-metal nanohybrid electrocatalyst for hydrogen evolution. Angew Chem Int Ed, 2014, 53: 6710–6714
18 Bao J, Zhang X, Fan B, *et al.* Ultrathin spinel-structured nanosheets rich in oxygen deficiencies for enhanced electrocatalytic water oxidation. Angew Chem Int Ed, 2015, 54: 7399–7404
19 Zhu YP, Liu YP, Ren TZ, *et al.* Self-supported cobalt phosphide mesoporous nanorod arrays: a flexible and bifunctional electrode for highly active electrocatalytic water reduction and oxidation. Adv Funct Mater, 2015, 25: 7337–7347
20 Yan Y, Xia BY, Ge X, *et al.* A flexible electrode based on iron phosphide nanotubes for overall water splitting. Chem Eur J, 2015, 21: 18062–18067
21 Gao X, Zhang H, Li Q, *et al.* Hierarchical $NiCo_2O_4$ hollow microcuboids as bifunctional electrocatalysts for overall water-splitting. Angew Chem Int Ed, 2016, 55: 6290–6294
22 Wang C, Jiang J, Ding T, *et al.* Monodisperse ternary NiCoP nanostructures as a bifunctional electrocatalyst for both hydrogen and oxygen evolution reactions with excellent performance. Adv Mater Interfaces, 2016, 3: 1500454
23 Jia X, Zhao Y, Chen G, *et al.* Ni_3FeN nanoparticles derived from

ultrathin NiFe-layered double hydroxide nanosheets: an efficient overall water splitting electrocatalyst. Adv Energ Mater, 2016, 6: 1502585
24 Xie X, Yu R, Xue N, *et al.* P doped molybdenum dioxide on Mo foil with high electrocatalytic activity for the hydrogen evolution reaction. J Mater Chem A, 2016, 4: 1647–1652
25 Balogun MS, Qiu W, Yang H, *et al.* A monolithic metal-free electrocatalyst for oxygen evolution reaction and overall water splitting. Energ Environ Sci, 2016, 9: 3411–3416
26 Xiao C, Li Y, Lu X, *et al.* Bifunctional porous NiFe/$NiCo_2O_4$/Ni foam electrodes with triple hierarchy and double synergies for efficient whole cell water splitting. Adv Funct Mater, 2016, 26: 3515–3523
27 Shi Y, Xu Y, Zhuo S, *et al.* Ni_2P nanosheets/Ni foam composite electrode for long-lived and pH-tolerable electrochemical hydrogen generation. ACS Appl Mater Interfaces, 2015, 7: 2376–2384
28 Pu Z, Liu Q, Asiri AM, *et al.* Tungsten phosphide nanorod arrays directly grown on carbon cloth: a highly efficient and stable hydrogen evolution cathode at all pH values. ACS Appl Mater Interfaces, 2014, 6: 21874–21879
29 Wang AL, Lin J, Xu H, *et al.* Ni_2P–CoP hybrid nanosheet arrays supported on carbon cloth as an efficient flexible cathode for hydrogen evolution. J Mater Chem A, 2016, 4: 16992–16999
30 Wang X, Li W, Xiong D, *et al.* Bifunctional nickel phosphide nanocatalysts supported on carbon fiber paper for highly efficient and stable overall water splitting. Adv Funct Mater, 2016, 26: 4067–4077
31 Pu Z, Liu Q, Jiang P, *et al.* CoP nanosheet arrays supported on a Ti Plate: an efficient cathode for electrochemical hydrogen evolution. Chem Mater, 2014, 26: 4326–4329
32 Yu M, Wang W, Li C, *et al.* Scalable self-growth of Ni@NiO core-shell electrode with ultrahigh capacitance and super-long cyclic stability for supercapacitors. NPG Asia Mater, 2014, 6: e129
33 Zou M, Jiang Y, Wan M, *et al.* Controlled morphology evolution of electrospun carbon nanofiber templated tungsten disulfide nanostructures. Electrochim Acta, 2015, 176: 255–264
34 Tan Y, Wang H, Liu P, *et al.* 3D nanoporous metal phosphides toward high-efficiency electrochemical hydrogen production. Adv Mater, 2016, 28: 2951–2955
35 Wang J, Zhong H, Wang Z, *et al.* Integrated three-dimensional carbon paper/carbon tubes/cobalt-sulfide sheets as an efficient electrode for overall water splitting. ACS Nano, 2016, 10: 2342–2348
36 Natile MM, Glisenti A. Surface reactivity of NiO: interaction with methanol. Chem Mater, 2002, 14: 4895–4903
37 Furstenau RP, McDougall G, Langell MA. Initial stages of hydrogen reduction of NiO(100). Surf Sci, 1985, 150: 55–79
38 Biesinger MC, Payne BP, Lau LWM, *et al.* X-ray photoelectron spectroscopic chemical state quantification of mixed nickel metal, oxide and hydroxide systems. Surf Interface Anal, 2009, 41: 324–332
39 Chigane M, Ishikawa M. XRD and XPS characterization of electrochromic nickel oxide thin films prepared by electrolysis–chemical deposition. Faraday Trans, 1998, 94: 3665–3670
40 Zou X, Huang X, Goswami A, *et al.* Cobalt-embedded nitrogen-rich carbon nanotubes efficiently catalyze hydrogen evolution reaction at all pH values. Angew Chem Int Ed, 2014, 53: 4372–4376
41 Vrubel H, Hu X. Molybdenum boride and carbide catalyze hydrogen evolution in both acidic and basic solutions. Angew Chem, 2012, 124: 12875–12878
42 Yang Y, Fei H, Ruan G, *et al.* Porous cobalt-based thin film as a bifunctional catalyst for hydrogen generation and oxygen generation. Adv Mater, 2015, 27: 3175–3180
43 Yan H, Jiao Y, Wu A, *et al.* Cluster-like molybdenum phosphide anchored on reduced graphene oxide for efficient hydrogen evolution over a broad pH range. Chem Commun, 2016, 52: 9530–9533
44 Shi J, Pu Z, Liu Q, *et al.* Tungsten nitride nanorods array grown on carbon cloth as an efficient hydrogen evolution cathode at all pH values. Electrochim Acta, 2015, 154: 345–351
45 Li J, Yan M, Zhou X, *et al.* Mechanistic insights on ternary $Ni_{2-x}Co_xP$ for hydrogen evolution and their hybrids with graphene as highly efficient and robust catalysts for overall water splitting. Adv Funct Mater, 2016, 26: 6785–6796
46 Shi J, Hu J. Molybdenum sulfide nanosheet arrays supported on Ti plate: an efficient hydrogen-evolving cathode over the whole pH range. Electrochim Acta, 2015, 168: 256–260
47 Son CY, Kwak IH, Lim YR, *et al.* FeP and FeP_2 nanowires for efficient electrocatalytic hydrogen evolution reaction. Chem Commun, 2016, 52: 2819–2822
48 Faber MS, Jin S. Earth-abundant inorganic electrocatalysts and their nanostructures for energy conversion applications. Energ Environ Sci, 2014, 7: 3519–3542
49 Faber MS, Dziedzic R, Lukowski MA, *et al.* High-performance electrocatalysis using metallic cobalt pyrite (CoS_2) micro- and nanostructures. J Am Chem Soc, 2014, 136: 10053–10061
50 Xie J, Zhang H, Li S, *et al.* Defect-rich MoS_2 ultrathin nanosheets with additional active edge sites for enhanced electrocatalytic hydrogen evolution. Adv Mater, 2013, 25: 5807–5813
51 Tian J, Liu Q, Cheng N, *et al.* Self-supported Cu_3P nanowire arrays as an integrated high-performance three-dimensional cathode for generating hydrogen from water. Angew Chem Int Ed, 2014, 53: 9577–9581
52 Peng Z, Jia D, Al-Enizi AM, *et al.* From water oxidation to reduction: homologous Ni-Co based nanowires as complementary water splitting electrocatalysts. Adv Energ Mater, 2015, 5: 1402031
53 Lukowski MA, Daniel AS, Meng F, *et al.* Enhanced hydrogen evolution catalysis from chemically exfoliated metallic MoS_2 nanosheets. J Am Chem Soc, 2013, 135: 10274–10277
54 Stern LA, Feng L, Song F, *et al.* Ni_2P as a Janus catalyst for water splitting: the oxygen evolution activity of Ni_2P nanoparticles. Energ Environ Sci, 2015, 8: 2347–2351
55 Fu G, Cui Z, Chen Y, *et al.* Ni_3Fe-N doped carbon sheets as a bifunctional electrocatalyst for air cathodes. Adv Energ Mater, 2017, 7: 1601172
56 Song F, Hu X. Exfoliation of layered double hydroxides for enhanced oxygen evolution catalysis. Nat Commun, 2014, 5: 4477
57 Yuan CZ, Jiang YF, Wang Z, *et al.* Cobalt phosphate nanoparticles decorated with nitrogen-doped carbon layers as highly active and stable electrocatalysts for the oxygen evolution reaction. J Mater Chem A, 2016, 4: 8155–8160
58 Feng LL, Yu G, Wu Y, *et al.* High-index faceted Ni_3S_2 nanosheet arrays as highly active and ultrastable electrocatalysts for water splitting. J Am Chem Soc, 2015, 137: 14023–14026

Acknowledgements This work was supported by the National Natural Science Foundation of China (21571073 and 21673090), the National Basic Research Program of China (2015CB932600), Hubei Provincial Natural Science Foundation of China (2016CFA031), the Program for HUST Interdisciplinary Innovation Team (2015ZDTD038) and the

Fundamental Research Funds for the Central Universities. The authors also thank the Analytical and Testing Center of HUST for the measurements.

Author contributions Li C performed the main experiments; Hou J participated in the characterization; Li C wrote the manuscript with support from Guo K, Wu Z, Wang D, Zhai T and Li H. All authors contributed to the general discussion.

Conflict of interest The authors declare that they have no conflict of interest.

Supplementary information Supporting data are available in the online version of the paper.

Caicai Li received her BSc degree from Anyang Normal University in 2013. She is now a PhD candidate at the School of Materials Science and Engineering, Huazhong University of Science and Technology (HUST). Her research is focused on the preparation of transition metal based nanomaterials for efficient water splitting.

Huiqiao Li received her BSc degree in chemistry from Zhengzhou University in 2003, and PhD degree in physical chemistry from Fudan University in 2008. Afterward, she worked as a postdoctoral fellow for four years at the Energy Technology Research Institute, National Institute of Advanced Industrial Science and Technology (AIST), Japan. Currently, she is a full professor at the School of Materials Science and Engineering, Huazhong University of Science and Technology (HUST). Her research interests include energy-storage materials and electrochemical power sources, such as lithium/sodium ion batteries, supercapacitors, and electrocatalysis.

酸活化法制备一体化镍/氧化镍电极用于碱性条件下分解水

李彩彩[1], 侯俊先[2], 吴则星[1], 郭凯[1], 王得丽[1], 翟天佑[1], 李会巧[1*]

摘要 开发和制备碱性条件下的非贵金属析氢和析氧催化剂对于缓解能源和环境危机至关重要. 本文利用一种简单的酸活化方法, 制备出了一种基于泡沫镍的镍/氧化镍一体化电极. 由于其粗糙及类片层的表面结构使得制备出的电极具有大的比表面积和更多的表面反应活性位点. 同时, 与粉末催化剂相比, 此一体化电极可实现催化剂和集流体之间的良好接触, 在一定程度上缓解催化剂的脱落问题, 保证了电极的稳定性. 当用作双功能催化剂时, 其表现出了优异的催化活性和良好的稳定性. 此法简单且易规模化, 可以为制备其他非贵金属催化剂提供思路.